Modeling and underwater characterization of cymbal transducers and arrays

J. Zhang, Anne-Christine Hladky, W.J. Hughes, R. Newnham

HAL Id: hal-00151690
https://hal.science/hal-00151690

Submitted on 28 Jul 2021

Modeling and Underwater Characterization of Cymbal Transducers and Arrays

Jindong Zhang, Anne-Christine Hladky-Hennion, W. Jack Hughes, *Member, IEEE*, and Robert E. Newnham, *Member, IEEE*

Abstract—The cymbal is a miniaturized class V flextensional transducer that was developed for potential use as a shallow water sound projector and receiver. Single elements are characterized by high Q, low efficiency, and medium power output capability. Its low cost and thin profile allow the transducer to be assembled into large flexible arrays. Efforts were made to model both single element and transducer arrays by coupling finite element analysis (ATILA) and the integral equation formulation (EQI). The pressure and velocity distributions on the surface elements were calculated by ATILA and later used with EQI to calculate the far field properties of the transducer element and arrays. It eliminates the mesh of the fluid domain and makes the 3-D model of a transducer possible. Three-dimensional models of a cymbal transducer and a 3 × 3 cymbal array were developed in the modeling. Very good agreement was obtained between modeling and measurement for single element transducers. By coupling finite element analysis with the integral equation method using boundary elements, acoustic interaction effects were taken into account. Reasonable agreement was obtained between calculation and measurement for a 3 × 3 array.

I. Introduction

THE CYMBAL transducers are miniaturized class V flextensional transducers. They consist of a piezoelectric disk (poled in the thickness direction) sandwiched between two "cymbal-shaped" metal end caps. The metal caps serve as a mechanical transformer that transform the high impedance, small extensional motion of the ceramic into low impedance, large flexural motion of the shell. The cymbal originally was designed as an actuator, which provides a sizable displacement as well as moderate generative force, bridging the gap between the two most common actuators, bimorph and the multilayer [1]. It was later proposed [2] as an underwater transducer for use as a sound projector and hydrophone. Because the cymbal transducer is small compared to the wavelength in water around resonance, it has modest radiation efficiency as a sound projector and a relatively high Q. It is necessary to assemble them into arrays to achieve the desired source level and directivity. In

assembling arrays, it always is desirable to have the transducer elements close packed in the array to save space. When element-to-element spacing is much smaller than the acoustic wavelength, acoustic interactions occur that lead to different acoustic loading on each transducer element, depending on its position in the array [3]. This then results in significant variations in the volume velocity of each array element. These interactions reduce the acoustic output power of the array and, in some extreme cases, a transducer element may have a negative radiation resistance and absorb acoustic power. However, the acoustic interaction leads to increased radiation resistance, therefore improving the radiation efficiency [4]. The acoustic loading effect is advantageous in the case of cymbal array because it improves the radiation efficiency.

The objective of this paper is to characterize the cymbal as an underwater transducer and attempt to model both single element and array by coupling finite-element analysis and the integral equation method.

II. Finite Element Modeling of an Underwater Transducer

The finite-element method has been used extensively in modeling complex transducer structures for more than 20 years. Many FEA software packages are commercially available, including ANSYS [5], PZFLEX [6], and ATILA [7]. The ATILA is specially designed for underwater transducers, which take into account the coupling between the transducer mechanical structure and the surrounding medium. In modeling underwater transducers, two approaches usually are used.

In the first method, a finite fluid domain is modeled in addition to the mesh of the solid structure, which is adapted from the ATILA code. Kinematic and dynamic continuity conditions are imposed at the interface for displacement and pressure fields. To absorb various components of the radiated field, damper elements are applied on the external surface Γ of the surrounding fluid domain [8]. The use of damper elements provides detailed information about the acoustic near field properties.

This method necessitates the modeling of the fluid domain, which in some cases leads to large meshes and is not well suited to 3-D modeling. A second method is to model only the solid structure using the finite element method, then couple it to an integral equation formulation to account for the acoustic radiation problems. In this way the

size of the mesh and the computation time can be significantly reduced [9]. By coupling the finite element and integral equation (EQI) methods, transducer arrays can be modeled.

The EQI is based on the Helmholtz-Kirchhoff Integral Equation, which is expressed as [10]:

$$\int\int \left\{ p(r')\frac{\partial G(r,r')}{\partial n'} - \frac{\partial p(r')}{\partial n'}G(r,r') \right\} dr' = \begin{cases} \alpha(r)p(r)/4\pi & r\epsilon\Gamma \\ p(r) & r\epsilon\Omega_f \end{cases} \quad (1)$$

where, $G(r,r') = \frac{1}{4\pi}\frac{e^{ik|r-r'|}}{|r-r'|}$ is the Green function. Γ is the external surface of the solid structure, Ω_f is the infinite fluid domain surrounding the solid structure, r is a point outside Γ, r' is a point on Γ, and $\alpha(r)$ is the solid angle at the point r.

The discretization of the integral equation on Γ consists of dividing the external surface of the structure into elements interconnected by nodes. On each element the pressure field and its normal derivative are connected to the nodal values by an interpolation function. Discretization leads to N equations with N unknowns, where N is the number of nodes in the grid. The matrix form of the system is:

$$[A]\{p\} = [B]\left\{\frac{\partial p}{\partial n}\right\}. \quad (2)$$

Matrices [B] and [A] come from the integration of the Green function, and their normal derivatives are computed by the interpolation functions. The vectors {p} and {$\partial p/\partial n$} contain the nodal pressures of the system and their normal derivatives. The displacement vector normal to the surface is given by:

$$\frac{\partial p(r)}{\partial n} = \rho\omega^2 u_n(r). \quad (3)$$

The solution of the linear systems provides the pressures at the nodes of the surface, from which the pressure at any point in the fluid Ω_f can be calculated.

In our approach, the solid structure is first meshed with special surface elements. Through harmonic analysis, the displacement and pressure field of the solid structure and the surface elements can be computed as a function of frequency using the finite element code ATILA. Then by enforcing kinematic and dynamic continuity conditions at the interface, the far field and near field pressures in the fluid domain are calculated with EQI.

III. EXPERIMENTAL PROCEDURE

A. Fabrication of the Cymbal Transducer and Array

The detailed fabrication procedure of cymbal transducer and arrays was described in a previously published paper [11]. The piezoelectric ceramic disks (PKI402,

Piezokinetics Inc., Bellefonte, PA) have a thickness of 1 mm and a diameter of 12.7 mm, and they were poled in the thickness direction. Titanium sheets of 0.25 mm thickness were used as the cap material. The shaped caps had a diameter of 12.7 mm. The cavity diameter was 9.0 mm at the bottom and 3.2 mm at the top. The cavity depth was 0.32 mm. Two different epoxy systems were used in this study. One is a high bonding strength insulating epoxy (Emerson and Cuming, Billerica, MA). A ratio of three parts 45 LV epoxy resin to one part 15 LV hardener was used. The other one is an E-solder conductive epoxy (Von-Roll ISOLA, New Haven, CT). In both cases, the thickness of the glue layer was approximately 40 μm. In the 3 × 3 array, the element center-to-center spacing was kept at 15 mm.

B. Characterization of the Cymbal and Arrays

Underwater calibration tests of single cymbals were performed at the Applied Research Laboratory, Penn State. The tank measured 5.5 m in depth, 5.3 m in width and 7.9 m in length. A pure tone sinusoidal pulse signal of 2-ms duration was applied to the test transducer, and its acoustic output was monitored with a standard F33 hydrophone. The test transducer and the standard were positioned at a depth of 2.74 m and separated by a distance of 3.16 m. The mechanical Q, transmitting voltage response (TVR), free-field voltage sensitivity (FFVS), and directivity pattern were evaluated.

In the underwater test, the cymbal transducer and array must be insulated from the conductive water in the tank. In addition, the array has to be rotated to observe the directivity pattern. A potting technique was devised for the transducer to maintain a mechanically free condition [11]. For single elements, a coaxial cable was first attached to the flange of the metal cap using silver epoxy. The cymbal and part of the cable then were potted in polyurethane with a thickness of about 0.5 mm. The polyurethane layer insulated the cymbal from the conductive water in the water tank. The 3 × 3 array was fixed at the end of a long plastic tube to allow rotation. The electrical lead wires passed through the plastic tube and were connected to the measurement system at the other end of the tube. The diameter of the tube is small compared to the wavelength in water so it does not interfere with the acoustic field generated by the array. The potted cymbal transducer and array are shown in Fig. 1.
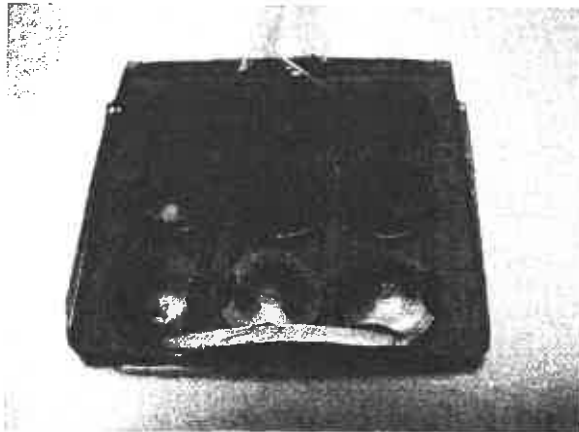
IV. RESULTS AND DISCUSSION

A. Single Element

Due to symmetry, only a quarter of the transducer structure was modeled. There are symmetry planes across XOY and XOZ. The mesh of the entire structure is too complicated to see any details; therefore, only the mesh of the surface element of the cymbal transducer is shown

(a) single element

(b) 3x3 array

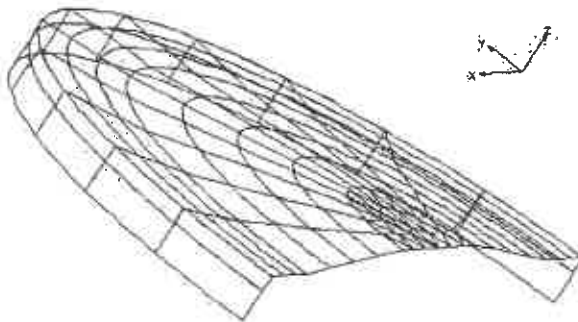Fig. 1. Photographs of a cymbal transducer and a 3 × 3 array potted in polyurethane.

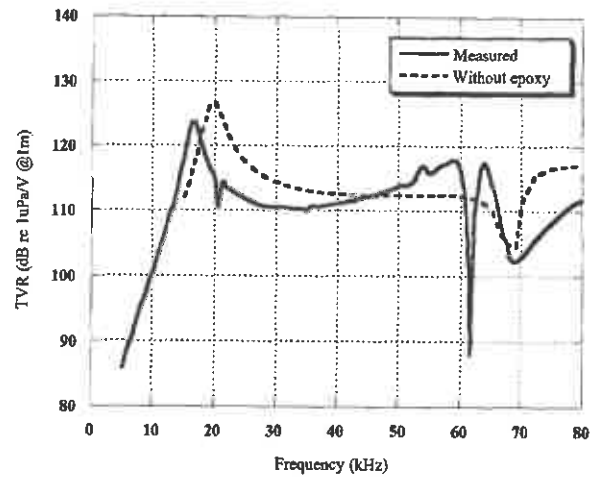Fig. 2. Mesh of the surface elements of a single element.

Fig. 3. Comparison of experimental and calculated TVR of a single element. Computation did not include the epoxy bonding layer.

in Fig. 2. The symmetry plane XOY is grounded and 1 V was applied to the upper side of the ceramic. Because 1 V was applied to a thickness of 0.5 mm, which is half of the thickness of the ceramic, the electric field was actually 1 V/0.5 mm = 2 V/mm. It is equivalent to an applied voltage of 2 V for a 1 mm-thick ceramic. Therefore, what the program calculates is source level (SL). To obtain the TVR, the following equation was used:

$$SL = TVR + 20 \ \log \ V. \qquad (4)$$

Here $20 \log V = 6$. Thus, we have to subtract 6 dB from the calculated source level to get TVR. For the same reason, the calculated impedance was multiplied by two to get TVR for a 1 mm-thick ceramic disk.

Because the epoxy thickness is very small compared with the ceramic and the caps, we initially did not include the epoxy layer in the model, assuming it has little effect on the transducer performance. Fig. 3 shows the calculated TVR of a cymbal transducer compared with measurement. Without modeling the glue layer, the calculated resonance frequency was about 20 kHz compared to the measured resonance frequency of 16.6 kHz. The considerable difference in resonance frequency suggests that the epoxy layer increases the effective compliance of the cymbal structure substantially. Therefore, the epoxy layer must be included in the model even at the cost of a larger mesh and considerably increased computation time.

In the next step, the epoxy layer was included in the modeling. Its thickness was assumed to be 40 μm. The calculated TVR is shown in Fig. 4 and compared with the measured values. A nearly perfect match was obtained over a wide frequency range from 10 kHz to 80 kHz. The four peaks at 20 kHz, 34 kHz, 53 kHz, and 62 kHz come from the resonance of the air bubbles in the cured polyurethane and will be ignored in the discussion. The major peak at 17 kHz in the TVR curve corresponds to the first flextensional mode of the caps, which is illustrated in Fig. 5(a).
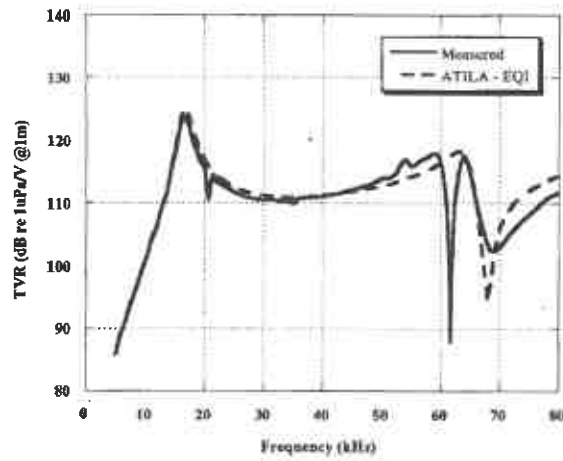
Fig. 4. Calculated and measured TVR of single cymbal modeled more accurately with the bonding layer.
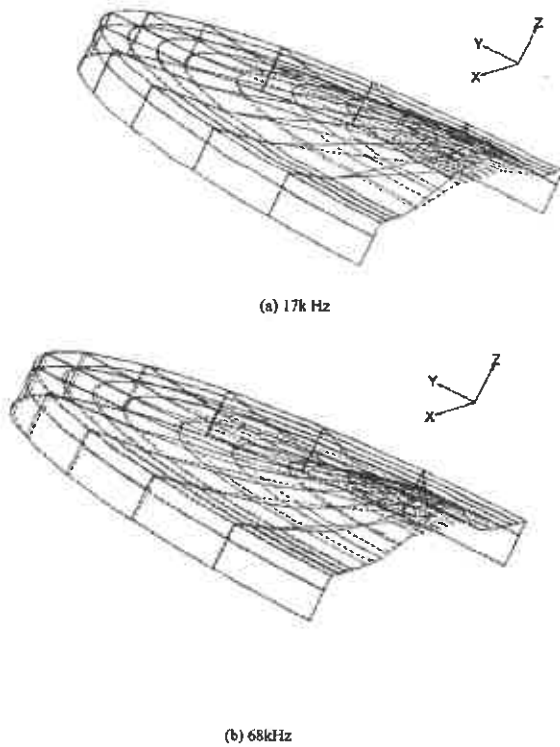

(a) 17k Hz

(b) 68kHz

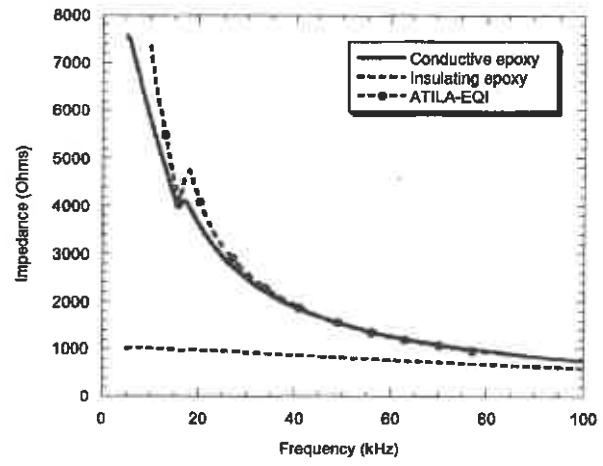Fig. 5. Displaced shape of the cymbal transducer at frequency: (a) 17 kHz, (b) 68 kHz.

Fig. 6. The calculated and measured impedance of a cymbal transducer.
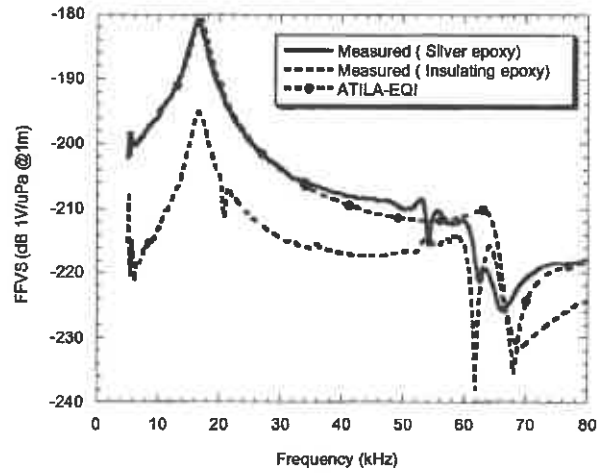

Fig. 7. Calculated FFVS of cymbal transducer based on reciprocity.

There is a sharp dip at about 68 kHz, which originates from the second flextensional mode of the metal caps. As seen from the vibration mode in Fig. 5(b) at this frequency, two portions of the cap vibrated out of phase. The pressures from different portions of the metal caps cancel out, leading to a sharp drop in transmit response.

The calculated impedance of a cymbal transducer is shown in Fig. 6 and compared with the measured impedance. There is a significant difference between the measurement and modeling at low frequencies. Based on reciprocity, the receive response of the cymbal transducer was calculated from the calculated TVR and impedance using the following equation:

$$TVR = FFVS + 20\log f - 20\log |Z| + 354. \quad (5)$$

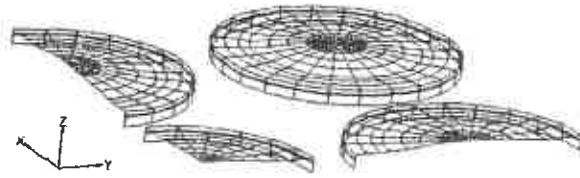Fig. 7 shows the calculated FFVS of a cymbal transducer compared with measurement. A difference of about

Fig. 8. Meshes of the surface elements of the 3 × 3 array. The center cymbal is in the lower left.

10 dB exists between the modeling and measurement. To explain the discrepancies, it is necessary to examine the experimental conditions. In the modeling, the electric field was applied directly to the face of the PZT disk, and it does not "see" the epoxy layer. In the measurement, the leads were connected to the cap instead of the PZT disk for convenience. The insulating epoxy layer sometimes can cause problems because of poor electrical contact. To verify this idea, another cymbal transducer of the same material and cap geometry was assembled with conductive epoxy. The electrical leads were connected to the flange of the cap in the usual way. The measured impedance and FFVS of the modified cymbal are shown in Fig. 6 and Fig. 7, respectively. In both cases, the modeling and measurement agree very well. It is clear now that poor electrical contact between the cap and ceramic is a weak point in the manufacture of a cymbal transducer. This problem can be solved by placing the epoxy layer under compressive stress, which is difficult to achieve experimentally and may complicate the design. Use of conductive epoxy can alleviate the problem by an order of magnitude. Unfortunately, the conductive epoxy usually has lower bonding strength and is not good for high power transmission. This is a materials problem requiring further attention.

B. Array Modeling

Three symmetry planes exist for the 3 × 3 array; therefore, only one-eighth of the array is modeled. Fig. 8 shows the mesh of the surface elements.

The predicted TVR of a 3 × 3 array with a center-to-center spacing of 15 mm is shown in Fig. 9 and compared with the measured TVR of the array. In both modeling and measurement, the peaks associated with the resonance have disappeared because of the damping associated with acoustic loading. This is a result of strong acoustic interaction between adjacent transducers at resonance. Although all the transducers in the array are electrically driven in phase, the amplitude and phase of the vibration of the transducers are very different, depending on their location in the array. The calculated displacement of the dome of transducers in the array is shown in Fig. 10 and compared with that of a single, individual element. At off-resonance frequencies, the displacement of transducers in the array is pretty much the same as that of a single element. At resonance, the displacement of the center transducer in the array is almost two times larger than that of a single, individual element at this frequency. Because of this
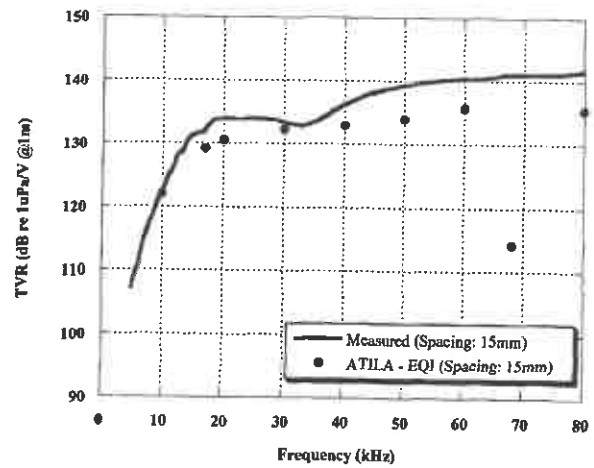

Fig. 9. Predicted TVR of a 3 × 3 cymbal array compared with measurement.
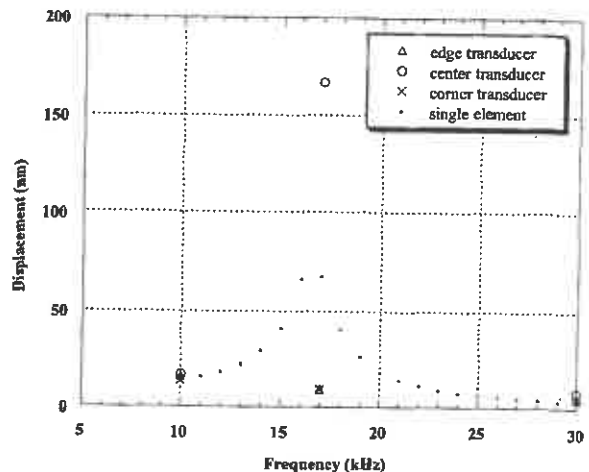

Fig. 10. Calculated displacement of transducers in the array and of a single, individual transducer.

large motion, the stress in the ceramic may exceed the mechanical tolerance and destroy the ceramic. In addition to mechanical failure, the heat generated in the ceramic due to mechanical and dielectric loss may depole the ceramic, leading to a thermal failure.

Fig. 11 shows the calculated displacement field of transducers in the array at the nominal resonance frequency (17 kHz). The corner transducers actually vibrate out of phase with the other transducers in the array. The pressures from different transducers partially cancel as a result of out of phase vibration. The net effect is, the resulting TVR curves are flattened around its nominal resonance and appear to have a broad band response.

Another consequence of array interaction is the improved efficiency of a 3 × 3 cymbal transducer array over
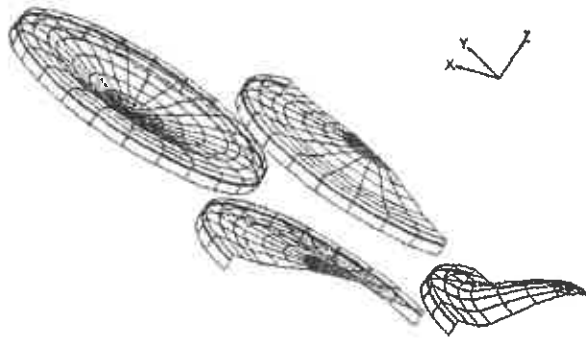
Fig. 11. The displacement fields of the transducer in the 3 × 3 array at 17 kHz (nominal resonance). The center cymbal is in the lower right.
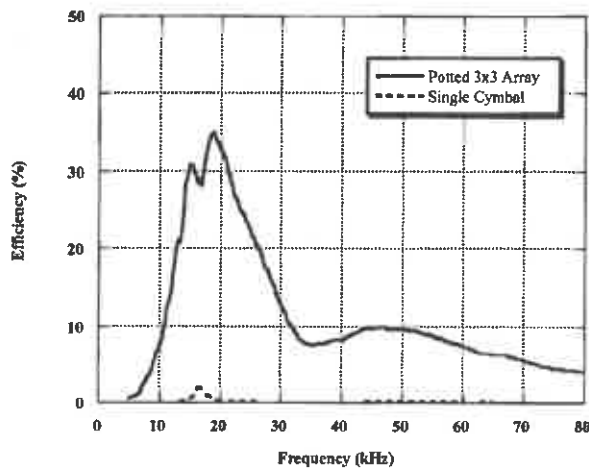

Fig. 13. The reduced motion of transducers in the array as a result of varying the surface geometry.

Fig. 12. Measured efficiency of a single cymbal transducer and of the potted 3 × 3 array.

Fig. 14. Predicted TVR of a 3 × 3 array of transducers with varied surface geometry compared with that of a 3 × 3 array with identical transducers.

an individual cymbal transducer. This is shown in Fig. 12. The array has an efficiency over 30% around nominal resonance, compared with the very small efficiency of the single cymbal transducer.

The calculations indicate that array interaction might be disastrous for a closely packed cymbal array driven at the nominal resonance, but there is a way to avoid this problem. Mutual radiation impedance not only depends on element-to-element spacing and operational wavelength, it also depends on the acoustic properties of the transducer surfaces and the shape of the transducer [3]. Instead of having identical transducers in the array, we slightly varied the cavity depth of the transducers in the array so that the surface geometry of the transducers was different. The cavity depth of the center transducer was maintained at 0.32 mm, and the cavity depths for the corner and edge transducers were 0.28 mm and 0.36 mm, respectively. Fig. 13 shows the calculated displacement of the dome area of the transducers in the array. At nominal resonance the displacement of the center transducer in the array was greatly damped
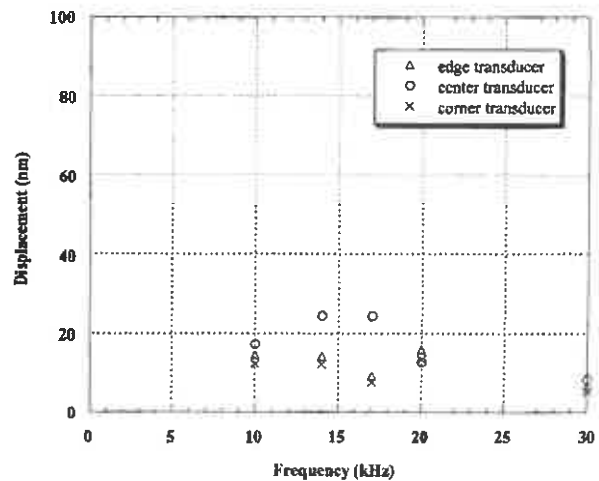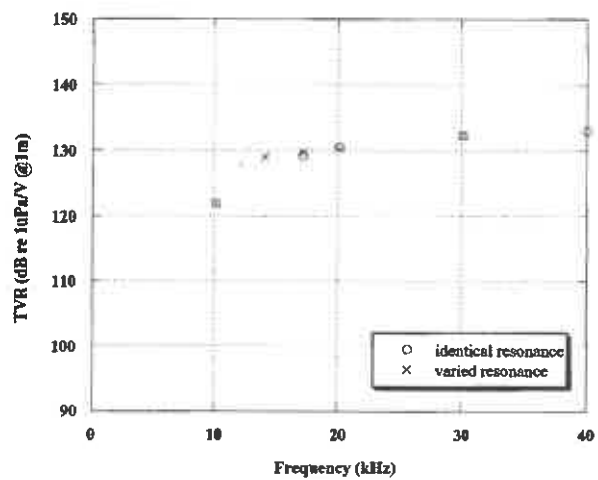
compared with its displacement in an array of identical transducers. It also is much smaller than that of a single, individual cymbal. Therefore, by slightly varying the surface geometry of the transducers in the array, the vibration velocities of the transducers in the array become more uniform, even at resonance, making the array less subject to the aforementioned mechanical and thermal failure. The predicted TVR of this array is nearly identical to the identical-transducer array shown in Fig. 14.

As shown in Fig. 9, the predicted TVR is 2 to 4 dB lower than the measured value above the nominal resonance frequency. This discrepancy is believed to be caused by the polymer matrix used in assembling the array. The potted array structure is actually very similar to the popular 1-3
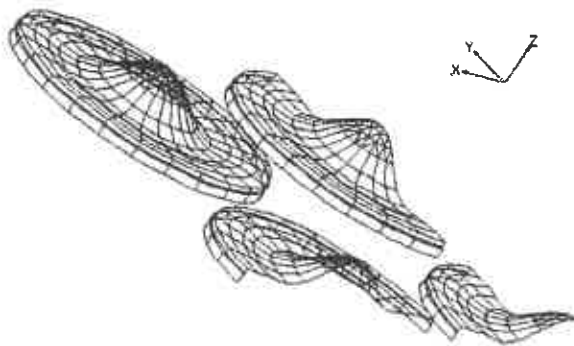
Fig. 15. Displacement field of transducers in the array at 68 kHz.

Fig. 16. Displacement field of transducers in the array at 80 kHz.

composite and has a similar decoupling effect [12] caused by the polymer matrix. As in the 1-3 composite, the radial motion of the ceramic disk is partially suppressed by the polymer matrix, and the axial motion of the caps is not. Therefore, the negative contribution of the radial motion to the sound pressure is reduced. Because the metal caps of the cymbal have an amplified motion in the axial direction, the effective acoustic impedance in the axial direction is reduced, and the polymer may further serve as a matching layer between the cap and water. Therefore, the energy transfer is more efficient in the axial direction than in the lateral direction of the array. The decoupling of the lateral motion of the ceramic from the axial motion and the improved acoustic matching layer increase the output pressure of the array.

The modeling predicts a sharp dip in the TVR curve for 3×3 array at 68 kHz, as shown in Fig. 9. This corresponds to the sharp dip in the TVR curve for a single element. The displacement pattern of the array at this frequency is illustrated in Fig. 15. At this frequency all the transducers have a similar vibration mode to that of a single element. Therefore, a dip in the TVR curve at this frequency is expected, but we did not observe such a dip in the measured TVR. Again, the discrepancy may be ascribed to the polymer matrix that alters the boundary conditions of the transducer elements in the array. Because the metal caps are in close contact with the polymer matrix, the two-nodal point line mode shown in Fig. 15 is not favorable and tends to be suppressed by the polymer matrix. As a result, the TVR is improved in this frequency range.

The vibration mode of transducers in the array at 80 kHz is shown in Fig. 16. The displacement for each transducer in the array is essentially the same with the same phase, suggesting little array interaction at this frequency as a result of large spacing to acoustic wavelength ratio at this frequency.

The calculated beam patterns of the 3×3 array in XOZ plane at various frequencies are shown in Fig. 17. The acoustic axis is the OZ direction. At frequencies up to 80 kHz, the modeling successfully predicts the main lobes and the side lobes in addition to the nulls in the beam pattern.
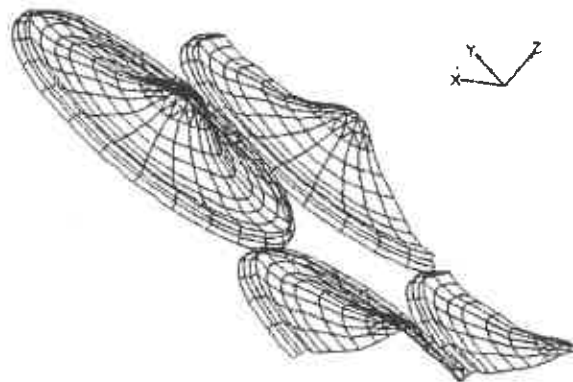
The effect of element center-to-center spacing in the array is shown in Fig. 18. At low frequencies when array interaction is severe, the predicted TVR is very sensitive to the element spacing. At the nominal resonance frequency of 17 kHz, the TVR of the array increases from 124 dB to 133 dB when the element spacing is increased from 13.5 mm to 16 mm. The difference is 9 dB when there is a change in spacing of only 2.5 mm. At higher frequencies, when the wavelength is of the same order of the size of the array (40 kHz), the predicted TVR is less dependent on the spacing.

V. SUMMARY

The coupling of finite element analysis and boundary element method provides an efficient way of modeling underwater transducers and arrays. For a single cymbal transducer, excellent agreement was obtained between calculation and measurement using this technique. The thin epoxy layer used to glue the caps to the ceramic disk has a tremendous effect on the transducer resonance and sensitivity. It is necessary to include the epoxy layer in finite element calculations, even at the cost of fine mesh and long computation time.

The acoustic interaction in the array was analyzed using the program EQI. The vibration modes of the transducers in the array behave very differently from a single, individual transducer at low frequencies where acoustic interaction is important. The vibration magnitude and phase of the transducers are strongly affected by the mutual radiation impedance, which is dependent on surface geometry of the transducers and their locations in the array. As the operational frequency increases, acoustic interaction becomes less severe, and transducers in the array behave more like a single, individual element. In addition to mutual radiation impedance, the vibration of the transducers in the array also is affected by the polymer matrix used in assembling the array. The polymer matrix tends to suppress the undesired vibration modes and improve the performance of the array. The combined finite element analysis and in-
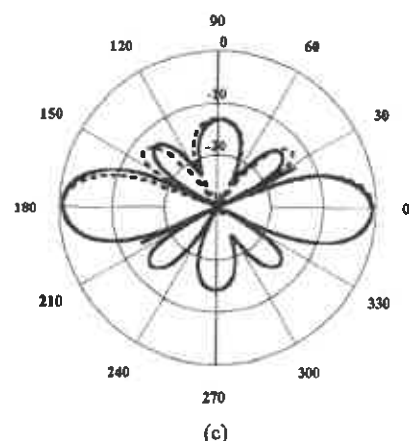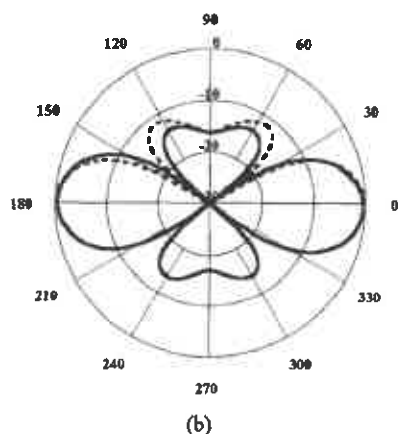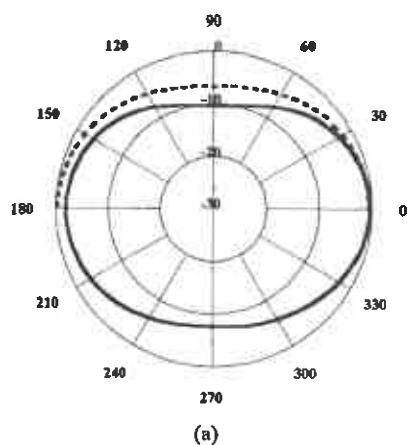
(a)

(b)

(c)

Fig. 17. Predicted beam patterns of the 3 × 3 array compared with the measured beam patterns (a) 20 kHz, (b) 60 kHz, (c) 80 kHz (— measured; - - - ATILA-EQI).
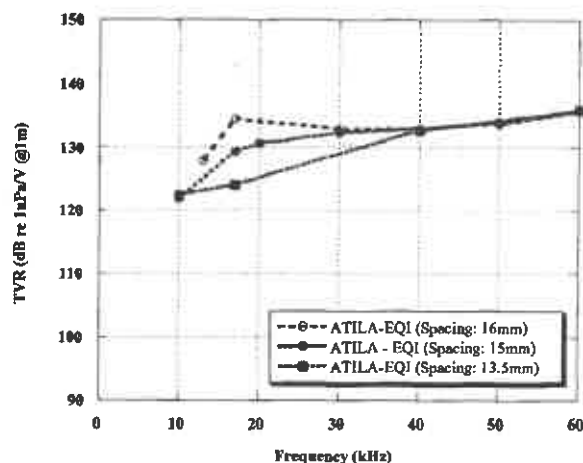
Fig. 18. Effect of element center-to-center spacing on the predicted TVR of a 3 × 3 array.

tegral equation method appear to be an effective way of modeling both single element transducers and arrays.

REFERENCES

[1] A. Dogan, K. Uchino, and R. E. Newnham, "Composite piezo-electric transducers with truncated conical endcaps 'Cymbals'," *IEEE Trans. Ultrason., Ferroelect., Freq. Contr.*, vol. 44, no. 3, pp. 597–605, 1997.

[2] J. F. Tressler, R. E. Newnham, and W. J. Hughes, "Capped ceramic underwater sound projector: The 'cymbal' transducer," *J. Acoust. Soc. Amer.*, vol. 105, no. 2, pp. 591–600, 1999.

[3] C. H. Sherman, "Analysis of acoustic interactions in transducer arrays," *IEEE Trans. Sonics Ultrason.*, vol. SU-13, no. 1, pp. 9–15, 1966.

[4] B. F. Hamonic, O. B. Wilson, and J.-N. Decarpigny, "The design of low-frequency underwater acoustic projectors: Present status and future trends," *IEEE J. Oceanic Eng.*, vol. 16, no. 1, pp. 107–121, 1991.

[5] SWANSON Analysis Systems, Inc., *ANSYS User's Manual*, Revision 5. Houston, PA: SWANSON Analysis Systems, Inc., 1992.

[6] N. N. Abboud, G. L. Wojcik, D. K. Vaughan, J. Mould, D. J. Powell, and L. Nikodym, "Finite element modeling for ultrasonic transducers," in *Proc. Int. Symp. Med. Imaging*, 1998, pp. 19–42.

[7] MAGSOFT Corporation, *ATILA Version 5.1X User's Manual*. Troy, NY: MAGSOFT Corp., 1997.

[8] B. Hamonic, J. C. Debus, J.-N. Decarpigny, D. Boucher, and B. Tocquet, "Analysis of a radiating thin-shell sonar transducer using the finite element method," *J. Acoust. Soc. Amer.*, vol. 86, no. 4, pp. 1245–1253, 1989.

[9] B. Stupfel, B. Lavie, and J.-N. Decarpigny, "Combined integral equation formulation and null-field method for the exterior acoustic problem," *J. Acoust. Soc. Amer.*, vol. 83, no. 3, pp. 927–941, 1988.

[10] ISEN, *EQI User's Manual.* France: ISEN, 1999.
[11] J. Zhang, W. J. Hughes, R. J. Meyer, Jr., K. Uchino, and R. E. Newnham, "Cymbal array: A broad band sound projector," *Ultrasonics*, vol. 37, pp. 523–529, 2000.
[12] K. A. Klicker, J. V. Biggers, and R. E. Newnham, "Composites of PZT and epoxy for hydrostatic transducer applications," *J. Amer. Ceram. Soc.*, vol. 64, no. 1, pp. 5–9, 1981.

Jindong Zhang was born in Nanyang, China on February 1, 1970. He received the B.S. degree in ceramic science and engineering in 1991 from Zhejiang University in China, and the M.S. degree in ceramic engineering in 1996 from Shanghai Institute of Ceramics, Chinese Academy of Sciences. He worked in Dalian Porcelain Insulator Works, China, as an engineer from 1991–1993.

He currently is a Ph.D. student in Intercollege Programs in Materials and The Pennsylvania State University, University Park, PA. His research interests are in electroceramics, piezoelectric actuators, and transducers.

Robert E. Newnham (M'85) was born in Amsterdam, NY, on March 28, 1929. He received the B.S. degree in mathematics in 1950 from Hartwick College, Oneonta, NY; the M.S. degree in physics from the Colorado State University, Fort Collins, CO; a Ph.D. degree in physics and mineralogy from The Pennsylvania State University; and a second doctorate in crystallography from Cambridge University in 1960.

He is ALCOA professor of solid state science and former Associate Director of the Materials Research Lab at The Pennsylvania State University, University Park, PA. His research interests are in structure-property relations, electroceramics, and composite materials for electronic applications.